Phase Behavior and Microstructure in Binary Block Copolymer/ Selective Solvent Systems: Experiments and Theory

Mårten Svensson,[†] Paschalis Alexandridis,[†,‡] and Per Linse*[,†]

Physical Chemistry 1, Center of Chemistry and Chemical Engineering, Lund University, P.O. Box 124, S-221 00 Lund, Sweden, and Department of Chemical Engineering, State University of New York at Buffalo, Buffalo, New York 14260-4200

Received August 17, 1998; Revised Manuscript Received December 7, 1998

ABSTRACT: A combined experimental and theoretical study of phase behavior and structure in binary systems of block copolymers and a selective solvent is presented. The block copolymers used here consist of poly(ethylene oxide) (PEO) and poly(propylene oxide) (PPO), and the solvent is water, selective for the PEO block. The concentration−temperature phase diagrams of $(EO)_8(PO)_{47}(EO)_8$ (Pluronic L92) and $(EO)_{11}(PO)_{70}(EO)_{11}$ (Pluronic L122) in water have been determined experimentally. These two block copolymers are unique in that they form both normal (H_1, "oil-in-water") and reverse (H_2, "water-in-oil") hexagonal lyotropic liquid crystalline structures in binary systems with water over the same temperature range. This is the first time the H_2 structure is reported in a binary PEO−PPO−PEO/water system. Thereafter, the predicted phase diagram of $(EO)_{20}(PO)_{69}(EO)_{20}$ in water is given, employing a self-consistent mean-field lattice theory with internal degrees of freedom. The free energy for a number of possible microstructures was calculated as a function of the polymer concentration, and the extensions of the one-phase and two-phase regions were established. The model predicted the composition and temperature stability ranges of disordered solution, micellar solution, normal hexagonal, lamellar, reverse hexagonal, and reverse cubic ordered phases which appeared at increasing $(EO)_{20}(PO)_{69}(EO)_{20}$ concentration, in good agreement with the experimental Pluronic L122 phase behavior. Moreover, the model provides the volume fraction profiles for the PEO, PPO, and water components in the self-assembled microstructures, information which is not readily accessible from experiments. Finally, an increased segregation among the species and an increased domain spacing at increasing polymer length were found. The data are consistent with the scaling behavior predicted for the domain size in weakly segregating block copolymer systems.

Introduction

Melts of block copolymers display ordered phases at a sufficiently strong segregation between the blocks, and the structure of the ordered phases is mainly governed by the volume ratio of the blocks.[1,2] The introduction of homopolymers into the melt[3] or the dissolution of block copolymers in a low molecular and selective solvent can lead to an even richer phase behavior.

Amphiphilic block copolymers of the poly(ethylene oxide)−poly(propylene oxide)−poly(ethylene oxide) (PEO−PPO−PEO) type, commercially available as Pluronic or Synperonic, are a class of block copolymers which have been extensively studied during the past decade.[4−7] In aqueous solution and at low concentration, they generally form micelles consisting of a core dominated by the hydrophobic PPO surrounded by a water-swollen PEO-rich corona, whereas at higher polymer concentration lyotropic liquid crystalline (LLC) phases normally are formed.[8−10] The binary phase behavior typically displays transitions from a disordered solution (with or without micelles, denoted here as L_1) to a highly viscous micellar cubic LLC phase (I_1), to a hexagonal LLC phase (H_1), and to a lamellar LLC phase (L_α) with increasing block copolymer concentration.

Moreover, the temperature has a strong impact on the properties of the PEO−PPO−PEO solution. The solubility in water of both PEO and PPO decreases with increasing temperature. The onset of the micellization is thus a function of both the PEO−PPO−PEO concentration and the temperature. The temperature at which the first micelles form, at a given block copolymer concentration, is known as the critical micellization temperature (cmt).[11] Upon a further temperature increase, the initially spherical micelles may become rodlike, and finally the aqueous block copolymer solution phase-separates into a concentrated polymer phase and a water-rich phase almost depleted in polymer. This temperature is the well-known cloud-point temperature (at that polymer concentration). In addition, thermoreversible transitions (thermotropic liquid crystallinity) exist in these systems: a temperature increase can cause a transition from, e.g., L_1 to H_1 and to L_α phase at the same concentration.[10]

The phase behavior of ternary systems (i.e., block copolymer/"water"/"oil", where "water" and "oil" are selective solvents) is even richer.[12−19] The presence of oil enables the formation of reverse (water-in-oil) phases, where the oil is the continuous phase, in addition to the normal ones (oil-in-water), where water is the continuous one. The concentration and temperature ranges over which the different phases form depend on (i) the block copolymer molecular weight, (ii) the block (EO/PO) ratio, and (iii) the solvent quantity and quality. PEO−PPO−PEO block copolymers thus allow great flexibility in attaining the desired structure under different conditions and can be viewed as model self-assembled systems.[19]

Recently, a theoretical study of the stability and relative location of LLC phases in binary phase diagrams of PEO−PPO−PEO block copolymers in water

* To whom correspondence should be addressed.
[†] Lund University.
[‡] State University of New York at Buffalo.

10.1021/ma9812940 CCC: $18.00
Published on Web 01/23/1999

was presented.[20] The calculations were carried out using mean-field theories employing either a continuum or a discrete space; both showed the following order of phase stability with increasing the polymer concentration: disordered (L_1) → close packed cubic (I_1) → normal cylindrical (H_1) → lamellar (L_α) → reverse cylindrical (H_2) → reverse close packed cubic (I_2) → disordered (L_2), which agreed qualitatively with the corresponding experimental phase diagrams. The decreased solubility of EO and PO segments upon temperature increase was modeled by using internal degrees of freedom of the polymer representing temperature-induced conformational changes of the (−O−C−C−O−) backbone.[21] This extension gives rise to thermotropic effects—at higher temperature, phases with high curvature (e.g., the close packed cubic phase) were destabilized and the repeating distance in the assemblies increased, in agreement with experimental findings.[8,10]

In this paper we examine experimentally and theoretically the phase behavior of asymmetric block copolymers in a selective solvent. We first present binary concentration−temperature phase diagrams for aqueous solutions of three PEO−PPO−PEO block copolymers (Pluronic L62, L92, and L122), having the same PEO content ratio (20%) but different molecular weights. The determination of the phase diagram of Pluronic L92 and L122 is new, whereas the one of Pluronic L62 is taken from ref 10. We then present a theoretical phase diagram based on the approach employed by Noolandi et al.[20] Free energy curves indicating the stability of the different phases were calculated for various concentrations and temperatures, and from these we constructed the phase diagram. The block copolymer in the model resembles Pluronic L122, and therefore a direct comparison between theoretical and experimental phase diagrams can be made. We also report on data from small-angle X-ray scattering and compare those with calculated domain spacings (repeating distance between the assemblies). Segment volume fraction profiles and scaling relations of the lamellar spacing, which are a direct outcome from the theory, are presented. Finally, the effects of increasing polymer molecular weight on the degree of phase separation and the domain spacing are discussed.

Experiments

Materials. The Pluronic L92 and L122 poly(ethylene oxide)-*b*-poly(propylene oxide)-*b*-poly(ethylene oxide) block copolymers were obtained as a gift from BASF Corp., Mount Olive, NJ, and were used as received (PLURONIC is a registered trademark of BASF Corp.). The L92 and L122 polymers have nominal molecular weights of 3650 and 5000, respectively, and 20 wt % PEO content (according to the manufacturer). On the basis of their molecular weights and chemical compositions, Pluronic L92 and L122 can be represented by the formulas $(EO)_8(PO)_{47}(EO)_8$ and $(EO)_{11}(PO)_{70}(EO)_{11}$, respectively. Deuterated water (D_2O) was obtained from Dr Glasser AG.

Determination of Phase Diagrams. Samples were prepared individually by weighing appropriate amounts of polymer and heavy water into 8 mm (i.d.) glass tubes that were flame-sealed immediately. The glass tubes with the samples were centrifuged repeatedly in both directions over a few days to facilitate mixing. During the time period required for homogenization, the samples were kept in a temperature-controlled room that was maintained at 25 ± 0.5 °C. Subsequently, they were left at a given temperature in a temperature-controlled bath or oven for several days to attain equilibrium. The samples were first examined for homogeneity by ocular inspection against scattered light. The boundaries between one-phase (transparent) and two-phase (nontransparent) regions were thus identified. Inspection between crossed polaroids distinguished between isotropic (nonbirefringent) phases such as micellar and nonisotropic (birefringent) phases such as lamellar and hexagonal. The structure of the various LLC phases was established from the reflections identified in SAXS spectra. It was thus possible from a systematic variation of the composition and the temperature and using the techniques outlined above to determine the phase boundaries with good precision (±0.5 wt %).

Structural Characterization Using Small-Angle X-ray Scattering (SAXS). SAXS measurements were performed on a Kratky compact small-angle system equipped with a position sensitive detector (see ref 10 for details). The obtained Bragg diffraction peaks are relatively sharp in which case no desmearing is required, and the correct peak position can be evaluated directly from the slit-smeared data.[10,12] The structure of the LLC phases was determined from the relative positions of the SAXS diffraction peaks. For the lamellar (smectic) and hexagonal (cylindrical assemblies crystallized in a two-dimensional hexagonal lattice) structures, the positions of the peaks should obey the relationships 1÷2÷3÷4... and 1÷√3÷2÷√7÷3..., respectively. The lattice parameters d (lamellar periodicity) and a (distance between the centers of adjacent cylinders) of the lamellar and hexagonal structures, respectively, were obtained from the position (q^*) of the first (and most intense) diffraction peak according to

$$\text{lamellar: } q^* = \frac{2\pi}{d}, \quad \text{hexagonal: } q^* = \frac{4\pi}{a\sqrt{3}} \qquad (1)$$

The parameters d and a will collectively be referred to as domain spacings.

Theory

Mean-field lattice theories were used to calculate the free energy of different phases of binary block copolymer/water solutions, and thereafter phase diagrams were constructed employing the relative stability of the phases. The free energy of disordered solutions without micelles were obtained by employing the Flory−Huggins lattice theory,[22,23] whereas the free energy calculations of disordered solution with micelles or the LLC phases were based on an extension of the Flory−Huggins theory to heterogeneous systems originally developed by Scheutjens and Fleer.[24] The model of the polymer segments possessed internal degrees of freedom to make it possible to describe the decreased solubility of EO- and PO-containing polymers in water with increasing temperature by employing a physical model developed by Karlström.[21] Briefly, the EO and PO segments are assigned with two conformational states each, one polar and one apolar. The population of the apolar state, with higher internal energy and higher statistical weight, is favored at higher temperature, whereas the polar state is favored at lower temperature. This will result in an unfavorable polymer−water interaction upon a temperature increase. This approach has successfully rationalized a number of different properties of different systems composed by EO- and/or PO-containing polymers in solution; see e.g. refs 20, 21, and 25−31.

Disordered Solution without Micelles. The Helmholtz free energy of mixing for a multicomponent and homogeneous system consisting of solvent(s) and polymer(s) with internal states can be expressed as[25,26]

$$\beta(A - A^*) = \beta(A_{\text{int}} - A_{\text{int}}^*) - \ln\frac{\Omega}{\Omega^*} + \beta(U - U^*) \qquad (2)$$

where A_{int} and U represent the internal free energy and

the configurational energy in the mixed system, respectively, while $\ln(\Omega/\Omega^*)$ is the mixing conformational entropy divided by the Boltzmann constant, and $\beta = 1/(kT)$, k being the Boltzmann constant and T the absolute temperature. Starred quantities denote corresponding quantities in a reference system where the components are in pure amorphous states. The internal free energy, the mixing configurational entropy, and the interaction energy are given by

$$\beta A_{\mathrm{int}} = \sum_x \sum_A n_x r_{Ax} \sum_B P_{AB}\left[\beta U_{AB} + \ln \frac{P_{AB}}{g_{AB}}\right]$$

$$\ln \frac{\Omega}{\Omega^*} = -\sum_x n_x \ln \frac{n_x r_x}{L} \qquad (3)$$

$$\beta U = \frac{1}{2}\sum_x \sum_A \sum_{A'} \sum_B \sum_{B'} n_x r_{Ax} P_{AB} \chi_{BB'} P_{A'B'} \phi_{A'}$$

Here r_{Ax} denotes the number of segments of type A (either water, EO, or PO) in component x (either water or PEO−PPO−PEO), r_x the total number of segments in component x (1 for water and >1 for PEO−PPO−PEO), n_x the total number of molecules of type x, L the total number of lattice sites, ϕ_A the volume fraction of species A, and $\chi_{BB'}$ the Flory−Huggins interaction parameter between species A in state B and species A′ in state B′. Moreover, P_{AB} is the fraction of species A in state B, U_{AB} the zero energy level of species A in state B, and g_{AB} the degeneration of species A in state B. In the case of EO (or PO), U_{AB} and g_{AB} describe the equilibrium between the polar and the nonpolar states of EO (PO). P_{AB} at equilibrium is given by eq 4 in ref 26. For given amounts of the components in the system $\{n_x\}$, we can now calculate the free energy of a homogeneous solution under the restriction $\sum_B P_{AB} = 1$ for all A.

Micellar Solution and Ordered Phases. We now allow for inhomogeneities of the different components in one direction, and segment density profiles are an outcome from the calculations. In the model employed here, the space between two reflective and planar surfaces (planar geometry) or within a reflective and curved surface (spherical or cylindrical geometry) is divided into M layers. The layers are numbered $i = 1, 2, ..., M$, starting from the midpoint of the two planar surfaces or from the center of the curved surface, respectively, and each layer has L_i sites. The random (mean-field) mixing is applied within each layer separately. The three terms describing the free energy in eq 2 are slightly different in the heterogeneous case. The total internal energy arising from the internal states becomes[25]

$$\beta A_{\mathrm{int}} = \sum_i \sum_A n_{Ai} \sum_B P_{ABi}\left[\beta U_{AB} + \ln \frac{P_{ABi}}{g_{AB}}\right] \qquad (4)$$

where U_{AB} and g_{AB} are the same as in the homogeneous case, $\sum_i$ is the sum over layers, n_{Ai} is the number of sites in layer i occupied by segments of type A, and P_{ABi} is the fraction of species A in layer i which is in state B (given by eq 6 in ref 25). The mixing entropy is given by[25]

$$\ln \frac{\Omega}{\Omega^*} = -\sum_x \sum_c n_{xc} \ln \frac{n_{xc} r_x}{\omega_{xc}} \qquad (5)$$

where n_{xc} denotes the number of chains of component x in conformation c and r_x the total number of segments in component x. ω_{xc} is related to the degeneration factor for component x in configuration x, which is given by eq A.1.2 in ref 25.

The total interaction energy between the different states is expressed as[25]

$$\beta U = \frac{1}{2}\sum_x^M L_i \sum_A \sum_{A'} \sum_B \sum_{B'} \phi_{Ai} P_{ABi} \chi_{BB'} \langle P_{A'B'i} \phi_{A'i} \rangle \qquad (6)$$

where A and A′ run over all species and B and B′ over all states. ϕ_{Ai} is the volume fraction of species A in layer i. In the case of nearest-neighbor interactions as applied here, $\langle ... \rangle$ indicates an average over the present and the two adjacent layers. From eqs 4−6 we may finally derive a species- and spatial-dependent potential u_{Ai} (given by eq 9 in ref 25), which depends on $\{\phi_{Ai}\}$.

To close the set of equations, we need to express the volume fraction profiles $\{\phi_{Ai}\}$ in terms of the potentials $\{u_{Ai}\}$. Such a relation can be derived on the basis of Boltzmann-weighted conformations, conserved chain connectivity across the layer boundaries, and fulfilled packing constraints (we again refer the reader to ref 25 for all the details). Hence, at this stage we now possess an implicit set of nonlinear equations for the segment distributions, which can be solved numerically.

Ordered Phases. The extension of the above theory to calculate the free energy, and thus the relative stability of the ordered phases, was given by Noolandi et al.[20] Briefly, at a given temperature, the free energy of each of the five ordered phases was calculated as a function of the composition of the system, $\{\phi_x\}$, and in each of the calculations the free energy was minimized with respect to the domain size (M). Such free energy curves [$A = f(\phi_{\mathrm{polymer}})$] were then repeatedly calculated for a set of different temperatures.

Micellar Solution. On the basis of the theory for heterogeneous system, we have determined the critical micelle concentration (cmc) and the free energy of a disordered micellar solution using a previously established procedure.[27,32] Briefly, the micellar solution is (hypothetically) divided into spherical subsystems (cells), which contain one micelle in the center surrounded by its accompanying solution. The excess free energy A_s of a subsystem consists of two parts: A^σ, which is associated with the formation of a micelle fixed in space in contact with a bulk solution, and the mixing entropy as given by

$$\beta A_s = \beta A^\sigma + \ln \frac{V_m}{V_s} \qquad (7)$$

where V_m and V_s are the volume of the micelle and the subsystem, respectively. A requirement for stable micelles at equilibrium is that a positive A^σ is balanced by a favorable micellar mixing entropy, implying that $A_s = 0$. Given that the equilibrium state and the segment distributions are determined, A^σ is obtained by

$$A^\sigma = A - A^* - \sum_x n_x(\mu_x - \mu_x^*) \qquad (8)$$

where $A - A^*$ is given by eqs 2 and 4−6 in the heterogeneous case, and $\mu_x - \mu_x^*$ denotes the difference between the chemical potential of component x in bulk and in the reference state (see eq 15 in ref 27). Moreover, the computation of the micellar solution properties involves the calculation of the excess number of component x, Γ_x, in the subsystem. From the excess number of components a micellar volume (V_m) is calculated. Equation 7 is then used to obtain the volume of the subsystem, V_s, and finally the total composition of the components is obtained according to $\phi_x = \Gamma_x/V_s + \phi_x^{bulk}$. Any change in the bulk compositions will lead to concomitant changes in the segment distribution and in the total concentration. The lowest polymer concentration at which stable micelles are formed (when $A^\sigma > 0$) is referred to as the cmc. (In this context, we neglect the possibility of micellar growth to rodlike micelles at increasing temperature. Such growth has previously been predicted using the same approach as used here.[28])

To compare the stability (free energies) between a disordered micellar solution and the ordered phases, the total free energy of the micellar subsystem, A_m, is needed. It was evaluated according to

$$A_m = \sum_{i=1}^{i_s} \sum_{x} (n_{xi} \mu_{x,i_s}) \qquad (9)$$

where n_{xi} is the number of segments belonging to component x in layer i and μ_{x,i_s} the chemical potential of component x determined from $\{\phi_{x,i_s}\}$ with $i_s = (3V_s/4\pi)^{1/3}$ and where i_s is not necessarily an integer.

Determination of Phase Diagram. Phase diagrams were constructed by using the free energy of the disordered micellar-free solution, of the disordered micellar-containing solution, and of the five ordered phases as a function of the composition and temperature. From the $A = f(\phi_{polymer})$ dependencies at one temperature, the composition ranges for one- and two-phase regions at that temperature were extracted by employing the double-tangent method graphically. This was repeated for different temperatures, and thereafter one-phase areas in the temperature−composition space were constructed.

To improve the precision of the locations of the one-phase areas (but without altering their boundaries), the free energies were modified according to

$$A_{mod} = (A - A^*) + (\lambda \phi_{polymer}) \qquad (10)$$

where λ is a factor suitably chosen for each tangent construction. The modified free energies were plotted vs the polymer concentration for the different phases, and then the double-tangent method was applied. An example of a such a construction is shown in Figure 1, where βA_{mod} for disordered phases without micelles and with micelles and for cubic, normal hexagonal, and lamellar LLC phases are given vs the polymer concentration at 29 °C. A tangent is drawn from the L_1'' solution to the L_α phase which predicts a two-phase region between $\phi_{polymer} = 0.12$ and 0.44. The modified free energies of the I_1 and H_1 phases exhibit higher values than the tangent and are therefore not stable phases at this condition. The free energy of the micellar solution phase is very concentration dependent as seen from the wedgelike shape of the free energy curve in Figure 1.

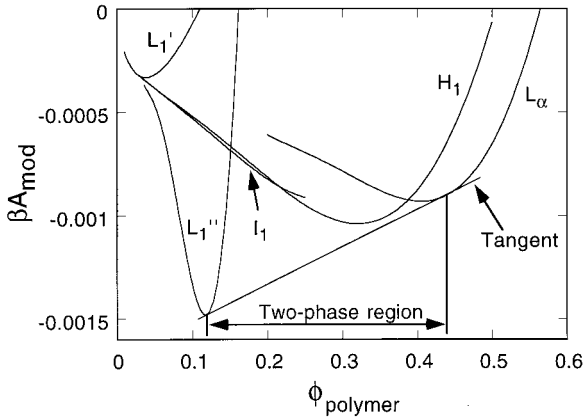

Figure 1. Modified free energies for different geometries (phases), βA_{mod}, vs block copolymer volume fraction at 29 °C. The determination of a two-phase region with the double-tangent construction is also shown. The following notation is used for the various phases: L_1', water-rich micellar-free disordered solution; L_1'', water-rich micellar-containing disordered solution; I_1, normal cubic LLC; H_1, normal hexagonal LLC; L_α, lamellar LLC.

Table 1. Internal State Parameters (U_{AB} and g_{AB}) and Flory−Huggins Interaction Parameters ($\chi_{BB'}$) of the Theoretical Model (Energy in kJ mol^{-1})

species	state	U_{AB}	g_{AB}
water		0	1
EO	polar	0[a]	1[a]
EO	nonpolar	5.086[a]	8[a]
PO	polar	0[b]	1[b]
PO	nonpolar	11.5[b]	60[b]

	$RT\chi_{BB'}$			
state	EO, polar	EO, nonpolar	PO, polar	PO, nonpolar
water	0.6508[a]	5.568[a]	1.7[b]	8.5[b]
EO, polar		1.266[a]	1.8[c]	3.0[c]
EO, nonpolar			0.5[c]	−2.0[c]
PO, polar				1.4[b]

[a] From the fit to the experimental PEO/water phase diagram.[21] [b] From the fit to the experimental PPO/water phase diagram.[25] [c] From the fit to the experimental PEO/PPO/water phase diagram.[26]

Polymer Model. We initially performed model calculations for $(EO)_{11}(PO)_{70}(EO)_{11}$ (Pluronic L122) in aqueous solution using interaction parameters taken from previous investigations. However, we failed to obtain a realistic phase diagram. However, an extension of the PEO block length facilitated the computation and produced much more realistic results. In the model calculations, $(EO)_{11}(PO)_{70}(EO)_{11}$ was replaced by $(EO)_{20}(PO)_{69}(EO)_{20}$, which corresponds to the nominal composition of Pluronic P123 (a block copolymer with the same PPO block length as the experimentally studied L122, but with a bit higher, 30%, PEO content). When investigating the polymer mass dependencies, polymers with the same EO/PO ratio as $(EO)_{20}(PO)_{69}(EO)_{20}$ were employed. The values of the parameters U_{AB}, g_{AB}, and $\chi_{BB'}$ were all taken from previous investigations and are given in Table 1, and thus no interaction parameters were adjusted in this study.

At the present status we have no clear explanation for the need of extending the length of the PEO blocks. Possible suggestions are (i) neglect of hydroxyl end groups of the Pluronic polymers (this effect increases as the length of the EO block is reduced), (ii) a too weak segregation between the PEO and PPO blocks, reflected

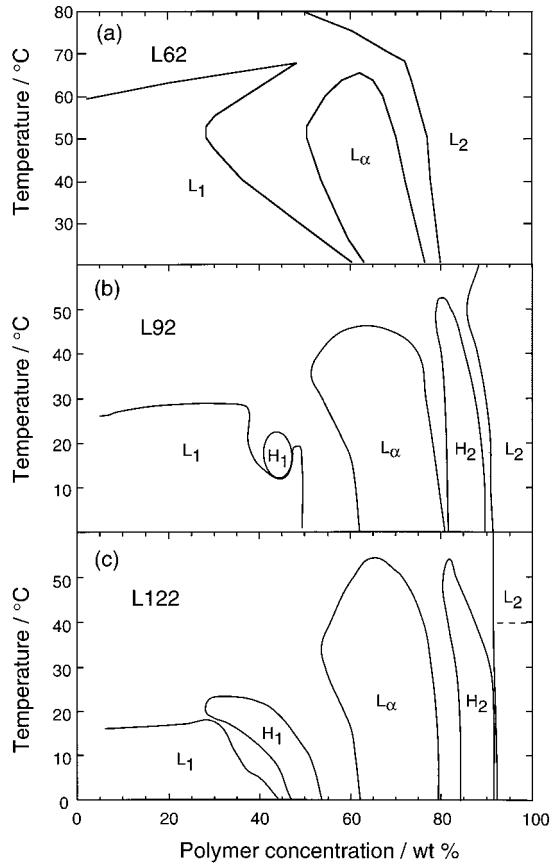

Figure 2. Experimentally determined concentration−temperature binary phase diagrams for the (a) Pluronic L62/water (adapted from ref 10), (b) Pluronic L92/water, and (c) Pluronic L122/water systems. The following notation is used for the various phases: L_1, water-rich disordered solution; H_1, normal hexagonal LLC; L_α, lamellar LLC; H_2, reverse hexagonal LLC; L_2, polymer-rich disordered solution. L62, L92, and L122 have the same EO/PO ratio but different molecular weight.

in the interaction parameters used, (iii) neglect of the mass and composition polydispersity as well as the presence of impurities appearing in the experimental systems, and, of course, (iv) effects of the approximations in the lattice theory used.

Results and Discussion

We will first consider the experimental phase diagrams of Pluronic L62, L92, and L122 in water and then the calculated one for $(EO)_{20}(PO)_{69}(EO)_{20}$. Thereafter, we will compare structural parameters obtained from SAXS measurements in the L122 system with the corresponding parameters resulting from the theoretical calculations. Finally, the volume fraction profiles of EO, PO, and water in the microstructures and scaling relations of the lamellar spacing, direct results of the calculations, are presented and discussed.

Phase Behavior. Figure 2 shows the experimentally determined phase diagram of aqueous solutions of Pluronic L92 and L122 for the whole concentration range and in the 0−60 °C temperature as well as the previously[10] determined one of Pluronic L62. The one-phase regions are enclosed by solid lines and are denoted (in order of increasing polymer concentration) L_1 (water-rich disordered solution), H_1 (normal hexagonal LLC), L_α (lamellar LLC), H_2 (reverse hexagonal LLC), and L_2 (polymer-rich disordered solution).

The same types of phases—L_1, H_1, L_α, H_2, and L_2—were obtained for Pluronic L92 and L122. Beginning at low polymer content, an isotropic solution region was found stable up to 45−50 wt % polymer and up to ∼28 °C (L92) and ∼16 °C (L122). The upper temperature limit corresponds to the cloud point of the polymer solution. With increasing the L122 polymer content, a narrow region of normal hexagonal LLC structure was obtained, which swelled to higher water concentrations (from 50 to 70 wt % water) when the temperature was increased from 0 to 20 °C (exhibiting a pronounced thermotropic effect). The hexagonal phase in the L92 system is stable over narrower concentration (42−47 wt % polymer) and temperature (12−22 °C) ranges. Moving to higher polymer contents, an extensive lamellar phase is obtained, separated from the H_1 phase by a fairly wide two-phase gap. The concentration range where the L_α structure is stable is similar (ca. 60−80 wt %) for both polymers (also for L62), but their temperature stability is a bit different. The L_α structure melts at 46 and 54 °C in the L92 and L122 systems, respectively. A common feature of both phase diagrams is that the concentration range over which the L_α is stable increases upon heating and displays a maximum at ≈35 °C.

Most notable is the observation of a reverse hexagonal H_2 phase, obtained in both the L92 and the L122 systems at high polymer concentrations (∼85−90 wt %), following the L_α region. The concentration and temperature stability range of the H_2 phase was similar in the two phase diagrams (i.e., independent of the polymer molecular weight), in contrast to that of the H_1 phase. The H_2 phase is stable up to ca. 54 °C in both phase diagrams. Its stability shifts to lower polymer content upon heating. This is the first time the H_2 structure is reported in a binary PEO−PPO−PPO/water system. Furthermore, these two block copolymers are unique among low molecular weight surfactants and lipids in that they form both normal (H_1, "oil-in-water") and reverse (H_2, "water-in-oil") hexagonal LLC structures in binary system with water in the same temperature range. Reverse structures are often found in ternary PEO−PPO−PEO/water/oil systems where the addition of oil increases the volume fraction of the apolar components (PPO and oil) and shifts the interfacial curvature toward "water-in-oil".[14,15,19] In the case of Pluronic L92 and L122, the high PPO content (80%) is adequate for forming a reverse (H_2) structure in the absence of oil. At the same time, the presence of 50% water is adequate (together with the polymer PEO content) to form the H_1 structure.

The formation of LLC structures in binary PEO−PPO−PEO/water systems and the concentration−temperature range of the stability of the different LLC structures depend on (i) the block copolymer molecular weight and (ii) the relative balance between the PEO and PPO blocks. First, a certain minimum molecular weight is required for the PEO and PPO blocks to segregate and to form LLC structures. For example, Figure 2a shows that the aqueous solution of Pluronic L62 displays only one LLC phase (a lamellar phase in the 62−77 wt % polymer range) as compared to the three LLC phases appearing in aqueous solutions Pluronic L92 and L122. Pluronic L62 has the same EO/PO ratio as L92 and L122, but a lower molecular weight (2200).

Second, the EO/PO ratio controls the structures formed. A high EO/PO ratio favors a curvature toward "oil-in-water", while a low EO/PO ratio favors the reverse structures. For example, an aqueous solution

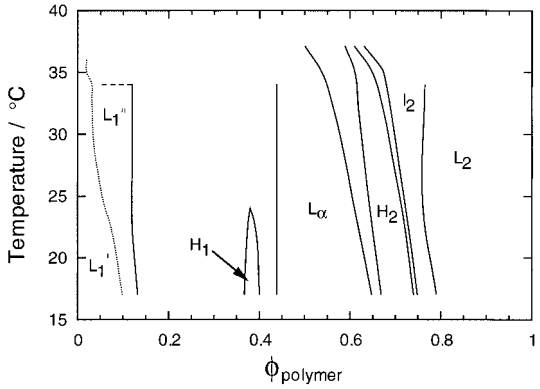

Figure 3. Calculated binary concentration−temperature phase diagram for $(EO)_{20}(PO)_{69}(EO)_{20}$/water system (solid lines represent one-phase boundaries). The notation is the same as in Figure 2, with the addition that the L_1' and L_1'' areas refer to water-rich disordered solution without and with micelles, respectively, separated by the critical micellization concentration (dotted line), and that I_2 denotes reverse micellar cubic LLC. The L_1'' phase ceases to exist above 34 °C, which is indicated by the dashed line.

of Pluronic F127 (70% EO content) forms an extended (20−65 wt % polymer) micellar cubic LLC phase with "oil-in-water" curvature.[17,18] However, in contrast to the case of a AB block copolymer melt, where mainly the A/B ratio controls the structure, in the present binary block copolymer−solvent systems the contribution of the solvent to the interfacial "curvature" has also to be considered.[14,15,19] As we see in the phase diagrams of Figure 2b,c, the same block copolymer can attain both normal (H_1, "oil-in-water") and reverse (H_2, "water-in-oil") hexagonal LLC structures in the presence of high (45%) and low (15%) water contents, respectively. In AB block copolymer melts, a similar change of phases requires polymers of different composition. Finally, when comparing with aqueous solutions of low molecular mass surfactants, the PEO−PPO−PEO macromolecules offer flexibility in attaining different structures that cannot be achieved in such systems.[19]

The calculated phase diagram for the aqueous solution of the $(EO)_{20}(PO)_{69}(EO)_{20}$ block copolymer (with a composition corresponding to that of Pluronic P123) is shown in Figure 3 and can be compared to the experimental L122 phase diagram (note that, for reasons of clarity, different temperature ranges are used in Figures 2c and 3). The one-phase areas are separated by two-phase regions (except for the two-phase region between I_2 and L_2 which is very narrow and is not displayed). The calculations predict stability of the following phases (in order of increasing polymer concentration): $L_1' + L_1''$ (water-rich disordered solution), H_1 (normal hexagonal LLC), L_α (lamellar LLC), H_2 (reverse hexagonal LLC), I_2 (reverse micellar cubic LLC), and L_2 (polymer-rich disordered solution). The dotted line at low polymer volume fraction indicates the location of the critical micellization concentration (cmc), being the border between L_1' (micelle-free disordered solution) and L_1'' (micelle-containing disordered solution), and it is clearly seen that the predicted cmc decreases with increasing temperature (in agreement with experiments[11]). The disordered phase in the calculated phase diagram ($L_1' + L_1''$) corresponds to the L_1 phase in the experimental L122 phase diagram.

The water-rich disordered solution (L_1) obtained in the calculated $(EO)_{20}(PO)_{69}(EO)_{20}$ system is narrow, reflecting a strong concentration dependence of the micellar free energy curve (see Figure 1). This is not in agreement with the experimental findings (Figure 2c) and may indicate that the model representing the micellar solution needs to be improved. At ca. 35 °C the L_1 phase becomes narrower and the two-phase region becomes even more extended, signaling the appearance of the clouding (macroscopic phase separation).

As seen in Figure 3, the I_1 phase (micellar cubic LLC) is not predicted to be stable, in agreement with the experimental L122 phase diagram. The H_1 phase is predicted to be stable and also very narrow (compared to the large L_α region), as found in the experimental L122 diagram; the location of the experimental H_1 region seems to be more influenced by temperature than that of the predicted H_1 shown in Figure 3. The extended L_α phase is superseded at higher polymer concentrations by H_2 and I_2 phases, separated by narrow two-phase regions. The concentration and temperature stability range of the predicted H_2 phase is in very good agreement with that of the experimental H_2 phase shown in Figure 2c. For instance, the H_2 phase becomes more stable at lower polymer concentrations upon heating and remains stable at higher temperatures than H_1. The predicted I_2 phase (reverse micellar cubic LLC) has not been observed experimentally; instead, the experiments show a L_2 phase (polymer-rich disordered solution) after the H_2 phase. However, polar domains have been identified in the L_2 phase of a binary PEO−PPO−PEO/water system.[16] The predicted I_2 structure is a reflection of such polar domains.

Thus, we notice that the experimental and predicted phase diagrams display strong similarities with respect to the existing phases, their structure, and their relative location. However, the agreement is still only qualitative as reflected by a number of details which still differ as well as a general shift in the polymer concentration of the appearance of the different phases. One of the differences is that the model tends to favor "water-in-oil" structures over the "oil-in-water" ones as evident from the necessity to increase the EO content of the triblock copolymer in the model and from the prediction of the existence of the I_2 phase.

Structural Characterization. SAXS measurements were performed for three compositions (two in the lamellar phase and one in the reverse hexagonal phase) of the L122 system at 25 °C. Figure 4 displays the scattering intensity. The domain spacings *d* and *a* were calculated from the first peak in the SAXS spectra using eq 1. Figure 5 shows the evaluated periodicities (filled symbols).

The calculated domain spacings from the model system at 24 °C are also given in Figure 5. To obtain real length units from the model predictions, we have used 4 Å for the length of a lattice cell, which has previously shown to give reasonable agreement with experimental data.[27,30] It is clearly demonstrated that the domain spacing decreases with increasing polymer concentration in the lamellar phase, a result from the decreased amount of water per block copolymer forming the interface. The concentration dependence on the repeating distance is the same for both experimental and calculated values in the L_α phase. However, the magnitude of the periodicity obtained from the model is about 40% too small (∼70 Å) as compared to the result from the experiment (∼115 Å). Calculations with a polydisperse polymer model[29] with a polydispersity ratio of 1.2 increase the repeating distance (to ∼85 Å) and

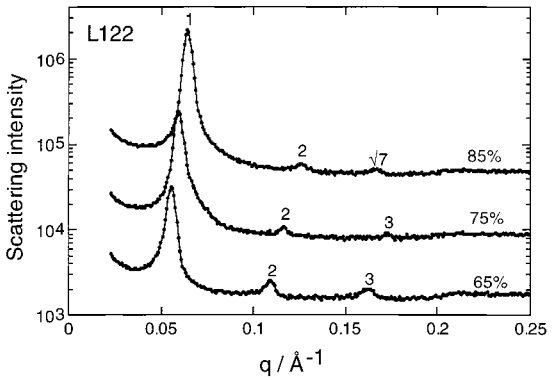

Figure 4. SAXS slit smeared diffraction patterns of the Pluronic L122/water (bottom) system at indicated polymeric weight compositions at 25 °C. The higher order 2 and 3 peaks were observed in the 65 and 75 wt % samples (indicative of lamellar structure), whereas the 2 and √7 peaks in the 85 wt % sample indicate hexagonal structure. [We have previously noticed that the intensity of the √3 peak may be small or the peak may disappear completely (as here), but the peak normally reappears for other compositions within the hexagonal phase.]

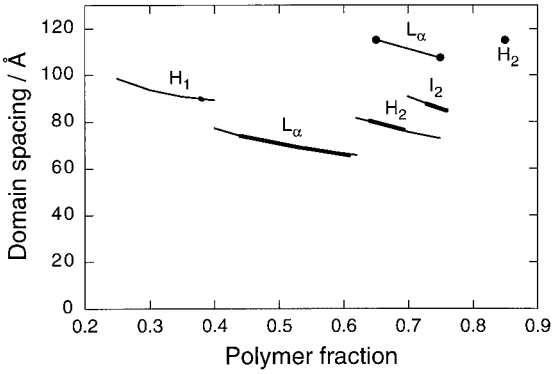

Figure 5. Domain spacing from SAXS measurements of aqueous solution of Pluronic L122 vs polymer fraction in wt % at 25 °C (filled circles) and from model calculations of aqueous solution of $(EO)_{20}(PO)_{69}(EO)_{20}$ vs polymer volume fraction at 24 °C (solid lines) at indicated ordered phases. Thick lines show stable one-phase areas as determined with the double-tangent method.

hence reduce a part of the discrepancy between the model calculations and the experimental data.

Also evident from Figure 5 is the decrease in domain spacing at the phase transitions when the curvature decreases, leading to the smallest spacing for the L_α phase. A curved interface implies an increased lateral expansion (and hence a reduced transverse extension) of the block(s) on the outside and a more transverse expansion of the other block(s). Obviously, the transverse expansion of the latter one(s) dominates.

Density Profiles. The volume fractions for each species (water, EO, and PO) in every lattice layer of the ordered phases are direct results from the theory. In Figure 6, density profiles are shown for the H_1 (normal hexagonal), L_α (lamellar), and H_2 (reverse hexagonal) structures. The extracted profiles are taken at 18 °C (H_1, L_α, H_2) and 33 °C (L_α, H_2) and at concentrations at which each phase is stable (see figure caption).

The hexagonal phase is narrow; thus, only one temperature profile is shown (Figure 6a). The center of the cylinder is dominated by a high concentration of PO species, $\phi_{PO} \approx 0.7$. The EO segments are to a large extent expelled from the PO-rich cylinders, and ϕ_{EO} displays a maximum outside the PO-rich cylinders.

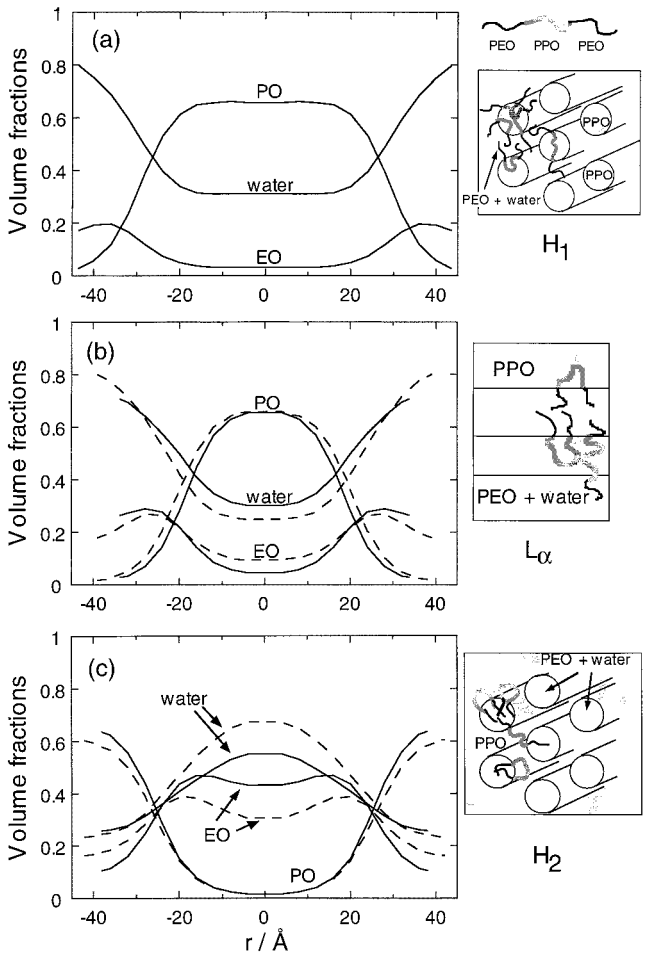

Figure 6. Calculated EO, PO, and water volume fractions profiles in the (a) normal hexagonal, (b) lamellar, and (c) reverse hexagonal phase for the $(EO)_{20}(PO)_{69}(EO)_{20}$/water system at 18 °C (full lines) and 33 °C (dashed lines). $\phi_{polymer}$ = 0.38, 0.50, and 0.67 for the normal hexagonal, lamellar, and reverse hexagonal phases, respectively.

Water is preferentially distributed outside the PO-rich cylinders, but an appreciable amount of water is predicted to be inside them. The predicted water content in the PO-rich region is probably too high, a feature previously found in the modeling of, e.g., lecithin bilayers.[33]

Figure 6b shows the density profiles for the lamellar phase. The gross features are the same as for the hexagonal phase, and the reduced transversal extension of the PPO blocks, leading to a narrower PO-rich region, is clearly visible (see also the discussion above). The altered segregation among the three species upon heating is demonstrated in Figure 6b. The volume fraction of water decreases in the PO-rich region and increases elsewhere, since PO becomes more hydrophobic at increasing temperature. EO also becomes more hydrophobic at increasing temperature, and its preference of water over PO is reduced as seen from the increased ϕ_{EO} in the PO-rich region. However, neither water nor the PO-rich region is ideal for EO, and hence the EO volume fraction profiles display a maximum between these two regions. It also evident in Figure 6b that the optimized domain spacing (repeating distance) increases upon temperature increase, which indicates that the interfacial area per PEO−PPO−PEO molecule is lowered due to the decreased solubility of the EO and PO blocks in water (this is in agreement with experimental observations[10]).

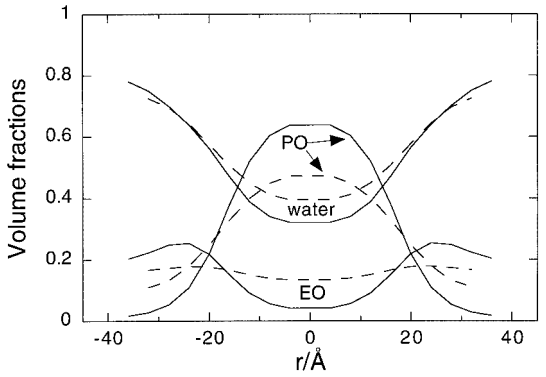

Figure 7. Calculated EO, PO, and water volume fractions profiles in the lamellar phase for the $(EO)_{20}(PO)_{69}(EO)_{20}$/water (full lines) and the $(EO)_{13}(PO)_{47}(EO)_{13}$/water (dashed lines) systems at 18 °C and $\phi_{polymer} = 0.45$.

The density profiles for the reverse hexagonal phase at 18 and 33 °C are shown in Figure 6c. Here, water reaches a high concentration in the interior of the cylindrical aggregates, whereas a high PO volume fraction is obtained outside them. The increased segregation between EO and water upon heating is pronounced; at the lower temperature the volume fractions of these two species are similar in the assemblies but differ significantly at the higher temperature. Again, the EO profiles display a maximum between the PO-rich and the water rich-regions. The domain spacing increases at higher temperature, but to a lower extent than in the lamellar case.

The effects of the block copolymer molecular weight on the phase behavior have been discussed above in connection to Figure 2. Here we turn our attention to the effects of molecular weight on the microstructure. Of particular interest is the degree of segregation between the polymer blocks. We can probe this with the help of the model and of experimentally determined domain spacings.

The effect of changing the molecular weight of the polymer on the density profiles is shown in Figure 7, where the volume fractions of water, EO, and PO in the lamellar phase are shown for two polymers [$(EO)_{20}(PO)_{69}(EO)_{20}$ and $(EO)_{13}(PO)_{47}(EO)_{13}$] having the same EO/PO ratio and at the same temperature and polymer volume fraction. Figure 7 clearly demonstrates that an increased molecular weight increases the segregation among the three species. For instance, at the lower molecular weight the EO fraction is nearly evenly distributed, while at the higher polymer weight EO attains distinct peaks between the PO-rich and water-rich regions. Moreover, ϕ_{PO} increases from 0.48 to 0.64 in the center of the aggregate upon increasing the molecular weight.

The increased segregation among the species at increasing molecular weight is further demonstrated in Figure 8. Here the EO and PO volume fractions in the center of the PO-rich region ($i = 1$) of the lamellar phase are plotted vs the number of polymer segments, for polymers with the same EO/PO ratio but with different length. At increasing molecular weight, the volume fractions of EO and PO decrease and increase, respectively, demonstrating an increased segregation between the species. For the shortest block copolymer shown, the segregation only appears between water and PO, which is a prerequisite for the existence of the ordered phases in these systems. At even shorter lengths, the disordered

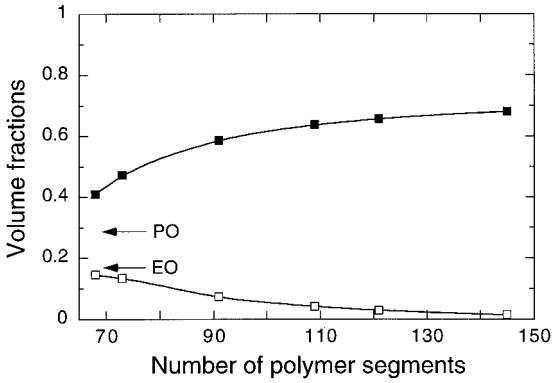

Figure 8. Calculated EO (open symbols) and PO (filled symbols) volume fractions in the center of the PO-rich region ($i = 1$) of the lamellar phase vs the number of polymer segments for $(EO)_{12}(PO)_{44}(EO)_{12}$, $(EO)_{13}(PO)_{47}(EO)_{13}$, $(EO)_{16}(PO)_{59}(EO)_{16}$, $(EO)_{20}(PO)_{69}(EO)_{20}$, $(EO)_{22}(PO)_{77}(EO)_{22}$, and $(EO)_{26}(PO)_{93}(EO)_{26}$, all having approximately the same EO/PO ratio, at 18 °C and $\phi_{polymer} = 0.45$. The arrows indicate the average volume fraction for each species.

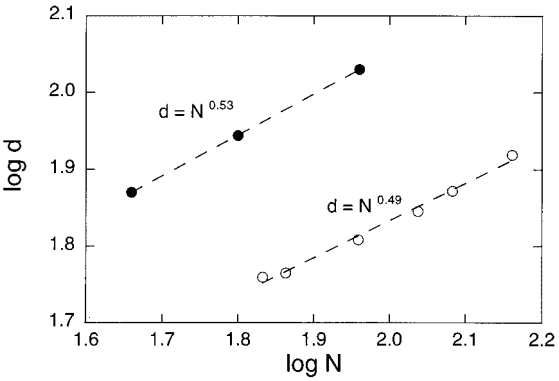

Figure 9. Logarithm of the lamellar domain spacing, *d*, vs the logarithm of number of polymer monomers, *N*, for aqueous solution of Pluronic L62, L92, and L122 from SAXS measurements at 25 °C at 75 wt % (filled symbols) and the corresponding calculated quantity vs the logarithm of number of polymer segments, *N*, for the block copolymers and conditions used in Figure 8 (open symbols).

state becomes the most stable one. At increasing polymer length, the water−PO segregation increases, and at the same time the EO starts to be expelled from the PO-rich region. At a length twice the one giving a stable lamellar phase, only a weak dependency of the EO and PO densities in the center of the PO-rich domain on the polymer length remains.

Finally, Figure 9 display the lamellar domain spacing vs the molecular weight at constant EO/PO ratio from SAXS measurements and model calculations. In this still narrow length interval, both the experimental and model data are consistent with a scaling relation $d = N^{\alpha}$, $\alpha \approx 0.5$. Moreover, the model data display a tendency to a stronger dependency (higher α) for longer polymers. Theoretically, the scaling relations with an exponent of $\alpha = 0.5$ for the weak segregation limit and $\alpha = {}^{2}/_{3}$ for the strong segregation limit has been obtained.[2] Hence, a comparison with our scaling exponents (from the experiments as well as the model) and the theoretical predictions indicates that our present system is in the weak segregation regime, which agrees with the relatively broad interfacial regions displayed in Figures 6 and 7. The relationship $d = N^{\alpha}$ has been experimentally observed also in ternary PEO−PPO−PEO/water/oil systems.[34]

Conclusions

A combined experimental and theoretical study of the phase behavior and the structure in binary systems of a block copolymer and a selective solvent is presented. The block copolymers used here consist of poly(ethylene oxide) (PEO) and poly(propylene oxide) (PPO), and the solvent is water, selective for the PEO block. The concentration−temperature phase diagrams of the binary $(EO)_8(PO)_{25}(EO)_8$ (Pluronic L92)/water and $(EO)_{11}(PO)_{70}(EO)_{11}$ (Pluronic L122)/water systems exhibited a number of lyotropic liquid crystalline phases: L_1 (unimer and micellar solution phase), H_1 (normal hexagonal), L_α (lamellar), H_2 (reverse hexagonal), and L_2 (disordered phase with high polymer content) with increasing block copolymer concentration. These asymmetric (20% PEO) block copolymers are unique in that they form both normal (H_1, "oil-in-water") and reverse (H_2, "water-in-oil") hexagonal lyotropic liquid crystalline structures in binary system with water at the same temperature range. This is the first time the H_2 structure is reported in a binary PEO−PPO−PEO/water system.

By using a self-consistent mean-field lattice model with internal degrees of freedom and independently determined interaction parameters, a corresponding phase diagram was calculated for $(EO)_{20}(PO)_{69}(EO)_{20}$ in water. The free energy for a number of possible microstructures, disordered and micellar solution, and ordered structures of spherical (cubic), cylindrical (hexagonal), and planar (lamellar) geometry was calculated as a function of the polymer concentration. Two-phase regions were determined from the free energy curves by the double-tangent method. The model predicted the composition and temperature stability ranges of disordered solution, micellar solution, normal hexagonal, lamellar, reverse hexagonal, and reverse cubic ordered phases (and their respective two-phase regions) with increasing $(EO)_{20}(PO)_{69}(EO)_{20}$ concentration, in agreement with the experimental Pluronic L122 phase behavior except for that the reverse cubic ordered phase is not present in the experimental system.

The model predicted the right composition dependence in d (the lamellar periodicity), but it underestimated its size. However, there is a certain ambiguity of converting lattice quantities, as the lattice size, to real units. Moreover, the model provided the volume fraction profiles for the EO, PO, and water components in the self-assembled microstructures, information which is not readily accessible from experiments. It was thus observed that the segregation between the different species became more pronounced upon heating, as a result of the decreased solubility of EO and PO in water at high temperatures. The domain spacing also increased with temperature, indicating an decrease in the interfacial area per block copolymer molecule. Finally, an increased segregation among the species and an increased domain spacing at increasing polymer length were found. The data were consistent with the scaling behavior predicted for the domain spacing in weakly segregating systems.

Acknowledgment. This work was financed by the Swedish Research Council for Engineering Science (TFR) and the Swedish National Research Council (NFR). P.A. thanks Karin Andersson for help in obtaining the experimental Pluronic L92 and L122 phase diagrams.

References and Notes

(1) Larson, R. G. *J. Phys. II* **1996**, *6*, 1441.
(2) Matsen, M. W.; Bates, F. S. *Macromolecules* **1996**, *29*, 1091.
(3) Janert, P. K.; Schick, M. *Macromolecules* **1997**, *30*, 137.
(4) Alexandridis, P.; Hatton, T. A. *Colloids Surf. A* **1995**, *96*, 1.
(5) Almgren, M.; Brown, W.; Hvidt, S. *Colloid Polym. Sci.* **1995**, *273*, 2.
(6) Chu, B.; Zhou, Z. In *Nonionic Surfactants: Polyoxyalkylene Block Copolymers*; Nace, V. M., Ed.; Marcel Dekker: New York, 1996; Vol. 60, p 67.
(7) Alexandridis, P. *Curr. Opin. Colloid Interface Sci.* **1997**, *2*, 478.
(8) Wanka, G.; Hoffman, H.; Ulbricht, W. *Macromolecules* **1994**, *27*, 4145.
(9) Zhang, K.; Khan, A. *Macromolecules* **1995**, *28*, 3807.
(10) Alexandridis, P.; Zhou, D.; Khan, A. *Langmuir* **1996**, *12*, 2690.
(11) Alexandridis, P.; Holzwarth, J. F.; Hatton, T. A. *Macromolecules* **1994**, *27*, 2414.
(12) Alexandridis, P.; Olsson, U.; Lindman, B. *Macromolecules* **1995**, *28*, 7700.
(13) Alexandridis, P.; Olsson, U.; Lindman, B. *J. Phys. Chem.* **1996**, *100*, 280.
(14) Alexandridis, P.; Olsson, U.; Lindman, B. *Langmuir* **1997**, *13*, 23.
(15) Alexandridis, P.; Holmqvist, P.; Lindman, B. *Colloids Surf. A* **1997**, *129−130*, 3.
(16) Caragheorgheopol, A.; Pilar, J.; Schlick, S. *Macromolecules* **1997**, *30*, 2923.
(17) Holmqvist, P.; Alexandridis, P.; Lindman, B. *Macromolecules* **1997**, *30*, 6788.
(18) Holmqvist, P.; Alexandridis, P.; Lindman, B. *J. Phys. Chem. B* **1998**, *102*, 1149.
(19) Alexandridis, P.; Olsson, U.; Lindman, B. *Langmuir* **1998**, *14*, 2627.
(20) Noolandi, J.; Shi, A.-C.; Linse, P. *Macromolecules* **1996**, *29*, 5907.
(21) Karlström, G. *J. Phys. Chem.* **1985**, *89*, 4962.
(22) Huggins, M. L. *J. Phys. Chem.* **1942**, *46*, 151.
(23) Flory, P. J. *J. Chem. Phys.* **1942**, *10*, 51.
(24) Fleer, G. J.; Cohen Stuart, M. A.; Scheutjens, J. M. H. M.; Cosgrove, T.; Vincent, B. *Polymers at Interfaces*; Chapman and Hall: New York, 1993.
(25) Linse, P.; Björling, M. *Macromolecules* **1991**, *24*, 6700.
(26) Malmsten, M.; Linse, P.; Zhang, K.-W. *Macromolecules* **1993**, *26*, 2905.
(27) Linse, P. *Macromolecules* **1993**, *26*, 4437.
(28) Linse, P. *J. Phys. Chem.* **1993**, *97*, 13896.
(29) Linse, P. *Macromolecules* **1994**, *27*, 6404.
(30) Linse, P.; Hatton, T. A. *Langmuir* **1997**, *13*, 4066.
(31) Svensson, M.; Linse, P. *Macromolecules* **1998**, *31*, 1427.
(32) van Lent, B.; Scheutjens, J. M. H. M. *Macromolecules* **1989**, *22*, 1931.
(33) Leermakers, F. A. M.; Scheutjens, J. M. H. M. *J. Chem. Phys.* **1988**, *89*, 3264.
(34) Alexandridis, P., to be published.

MA9812940